Retraction

Retracted: Construction and Validation of a CNV-Driven Ferroptosis-Related Gene Signature for Predicting the Prognosis of Lung Adenocarcinoma

Journal of Sensors

This article has been retracted by Hindawi following an investigation undertaken by the publisher [1]. This investigation has uncovered evidence of one or more of the following indicators of systematic manipulation of the publication process:

(1) Discrepancies in scope

(2) Discrepancies in the description of the research reported

(3) Discrepancies between the availability of data and the research described

(4) Inappropriate citations

(5) Incoherent, meaningless and/or irrelevant content included in the article

(6) Manipulated or compromised peer review

The presence of these indicators undermines our confidence in the integrity of the article's content and we cannot, therefore, vouch for its reliability. Please note that this notice is intended solely to alert readers that the content of this article is unreliable. We have not investigated whether authors were aware of or involved in the systematic manipulation of the publication process.

In addition, our investigation has also shown that one or more of the following human-subject reporting requirements has not been met in this article: ethical approval by an Institutional Review Board (IRB) committee or equivalent, patient/participant consent to participate, and/or agreement to publish patient/participant details (where relevant).

Wiley and Hindawi regrets that the usual quality checks did not identify these issues before publication and have since put additional measures in place to safeguard research integrity.

We wish to credit our own Research Integrity and Research Publishing teams and anonymous and named external researchers and research integrity experts for contributing to this investigation.

The corresponding author, as the representative of all authors, has been given the opportunity to register their agreement or disagreement to this retraction. We have kept a record of any response received.

References

[1] Y. Wang, Y. Zhao, Y. Li, Z. Luo, and H. Chen, "Construction and Validation of a CNV-Driven Ferroptosis-Related Gene Signature for Predicting the Prognosis of Lung Adenocarcinoma," *Journal of Sensors*, vol. 2022, Article ID 6883739, 15 pages, 2022.

Hindawi

Research Article

Construction and Validation of a CNV-Driven Ferroptosis-Related Gene Signature for Predicting the Prognosis of Lung Adenocarcinoma

Yanqing Wang [1], **Yi Zhao** [2], **Yong Li**,[1] **Zemin Luo**,[1] **and Hongzhu Chen**[1]

[1]*Integrated Chinese and Westeern Treatment of Oncology Dept, Central Hospital of Guangdong Provincial Nongken, No. 2,
Middle Renmin Road, Xiashan District, Zhanjiang City, Guangdong Province MO 524000, China*
[2]*Guangdong Ocean University No. 1, Haida Road, Mazhang District, Zhanjiang City, Guangdong Province MO 524088, China*

Correspondence should be addressed to Yi Zhao; zhaoyi@gdou.edu.cn

Background. Previous studies have shown that ferroptosis plays an integral role in the development of cancer and copy number variations (CNVs) have been reported to associated with the ferroptosis. However, the role of CNVs-driven ferroptosis-related genes (FRGs) in lung adenocarcinoma (LUAD) continues to be poorly understood. Therefore, we aimed to establish a novel gene signature in LUAD based on CNVs-driven ferroptosis-related genes. *Methods*. The transcriptome data and clinical features of LUAD patients were downloaded from the Gene Expression Omnibus (GEO) database and The Cancer Genome Atlas (TCGA) database. Differential analysis was carried out to recognize differentially expressed CNV-driven FRGs. Univariate Cox and least absolute shrinkage and selection operator (LASSO) regression analyses were utilized to identify prognosis-associated genes. Kaplan-Meier (K-M) analysis was a builder to estimate the worth of model. In addition, the nomogram was created to estimate survival probability of each patient. Ultimately, the immune microenvironment landscape between high and low risk groups was evaluated. *Results*. A total of 22 differentially expressed CNV-driven FRGs were acquired in LUAD. These genes were significantly associated with serine family amino acid metabolism, iron regulation, reactive oxygen species metabolism, and cellular response to oxidative stress, and were involved in amino acid metabolism, malaria, amino acid biosynthesis, and HIF-1 signaling pathways. Moreover, on the strength of 6 genes (TFAP2A, SLC2A1, AURKA, CDO1, SLC7A11, and ALOX5), the prognostic model was created, and the LUAD samples were significantly fall into the high- and low-risk groups, with the high-risk group had a poorer prognosis. Furthermore, risk score was an independent prognostic element. The nomogram with excellent predictive performance was developed for calculating the final result of LUAD patients at 1, 2, and 3 years. Finally, 19 immune cells had different infiltration differences among groups. *Conclusion*. A novel CNV-driven ferroptosis-related prognosis was established and could be used as a predictive indicator in LUAD. However, further clinical and in vivo in vitro experiments are necessary.

1. Introduction

On the basis of the Global Cancer Statistics 2018 [1], lung cancer is a disease and has the highest morbidity and mortality in China. The dominant type of lung cancer is non-small cell lung cancer (NSCLC), which more than 85%, along with lung adenocarcinoma (LUAD) that is the most frequent subtype of NSCLC [2]. The 5-year serial of most LUAD patients is less than 15% because of the lack of early diagnosis and post-diagnosis bio-

markers [3]. In addition, by reason of the high heterogeneity and complexity of lung cancer, there are significant differences in survival between LUAD patients with different molecular subtypes [4]. Despite considerable advances in chemotherapy, radiation, and targeted therapies for LUAD, survival rates for patients with the LUAD still received a poor prognosis [5]. Therefore, new sensitive biomarkers are starved for evaluate the prognosis of patients with LUAD at an early stage, which is especially critical for the prognosis and treatment of patients.

Ferroptosis is a form of iron-dependent cell death process activated by the accumulation of lipid peroxidation (LPO), which is different in cell necrosis, apoptosis and autophagy [6, 7]. There are reactive oxygen species (ROS) along with lipid oxidation markers in lung cancer tissues, suggesting ferroptosis may exist in lung cancer cells. Jiang et al. [8] showed that p53 is an important pathway for inducing ferroptosis to interrupt the growth of lung cancer, so ferroptosis play vital function in the tumorigenesis. In recent years, ferroptosis inducer inhibitors were also proved to have potential antitumor ability [9, 10]. Therefore, ferroptosis-related genes (FRGs) have hopes to turn into the future fresh targets for the LUAD manage.

Copy number variation (CNV) is part and parcel of genome structural variation, which is a DNA fragment variation between 1 kB and 3 Mb in size, including deletion, duplication, inversion, and translocation [11]. The amplification or deletion of copy number in cancer genome usually leads to the activation of proto-oncogene with tumor suppressor, which eventually brings about the occurrence of tumor [12]. Previous research has verified that CNV is key factor affecting patient outcomes, and characteristic CNV can play a role to judge the prognosis of cancer patients. For example, it was reported that CNV of DICER1 and DROSHA is closely related to the NSCLC patient's outcome, in which the upregulation expression of DROSHA becomes weak the survival, while the increased expression of DICER1 increases the survival [13]. Sriram et al. [14] found that the drop of copy number and decreased expression of SOCS6 were carefully bound up with the recurrence of LUSC. Liu et al. [15] found that CNV of TERT with PBX1P1 was related to the development of LUAD. CNV-driven FRGs have rarely been reported in LUAD. Therefore, this paper mainly constructed and verified the prognostic model with LUAD according to CNV-driven ferroptosis genes and analyzed the prognostic characteristic genes, which is helpful to fundamentally comprehend the role of CNV-driven ferroptosis genes in the progression of LUAD.

In view of relevant data of LUAD in TCGA database and GEO database, a six-gene prognostic model was structured in the present investigation, including TFAP2A, SLC2A1, AURKA, CDO1, SLC7A11, and ALOX5, through a series of bioinformatics techniques. After that, survival analysis proved the prognostic capability of six CNV-driven FRGs. As expected, in the TCGA training set, the analysis shows that CNV-driven FRG is associated clearly with OS of patients in the internal validation set as well as the external validation set. Besides, univariate and multivariate Cox independent prognostic analysis suggests that the risk score has the capacity to independently forecast patient survival. A nomogram with excellent predictive performance was developed for predicting the outcome of LUAD patients at 1, 2, and 3 years. Further analysis of immune cells and immunotherapy in two different hazard groups found the significant differences in 19 types of immune cells. Therefore, the prognostic model constructed in our present investigation exhibits superior predictive value, which can help clinicians make the best clinical policy with enhance OS rate of LUAD patients.

2. Materials and Method

2.1. Data Source. Transcriptome data (Level 3) and appropriate clinical messages of the LUAD were acquired from The Cancer Genome Atlas (TCGA) database (https://tcga-data.nci.nih.gov/tcga/), including 479 LUAD samples with fully available survival data, 56 LUAD samples with unavailable survival LUAD data, and 59 normal tissue samples. The TCGA-LUAD dataset shows the gene-level transcription estimates, as in $\log2(x+1)$ transformed RESM normalized count. In addition, a total of 1147 copy number variation (CNV) material were obtained from the TCGA database (normal = 591 and LUAD = 556). Moreover, transcriptome sequencing data of 442 LUAD samples with fully available survival data in the GSE68465 dataset was procured and acted as a validation cohort from the Gene Expression Omnibus (GEO) database (http://www.ncbi.nlm.nih.gov/geo/). Sixty FRGs were gained from the accepted literature,which were presented in Supplementary file 1. Ferroptosis-related driver and suppressor with tagging genes were from the FerrDb database.

2.2. Identification of Differentially Expressed CNV-Driven FRGs in LUAD. The differentially expressed genes (DEGs) in 535 LUAD with 59 control samples from TCGA-LUAD cohort were determined by "limma" package (version 3.46.0) with P value less than 0.05 with $|\log 2 FC|$ greater than or equal 0.5. The principal component analysis (PCA) was performed in the TCGA-LUAD according to the DEGs employing the "FactoMineR" (version 2.4) and "factoextra" package (version 1.0.7). The CNV region of genes was commented by employing the reference genome Research Consortium Human build 38 (GRCh38). The gene copy variation rates in control and patient samples were then analyzed, and genes with P value less than 0.05 were selected as CNV driver genes. The CNV driver genes and DEGs were intersected to obtain differentially expressed CNV driver genes. Moreover, a total of 397 FRGs were collected from previous study and ferrdb database. Then, correlation analysis between FRGs and differentially expressed CNV driver genes was performed to screen CNV-driven ferroptosis genes ($|\text{cor}| > 0.6$ and $P < 0.05$), which were taken to intersect with DEGs as differential CNV-driven ferroptosis-related genes.

2.3. Functional Enrichment Analysis. To further explore the functions of DEGs and differential CNV-driven ferroptosis-related genes, enrichment analysis was performed on the grounds of the Gene ontology (GO) and Kyoto Encyclopedia of Genes and Genomes (KEGG) databases to find common functions with correlative pathways by using "clusterProfiler" package. The screening criteria were $P < 0.05$ and counts ≥ 2. Use "enrichplot" (version 1.10.2) to plot bar graphs to display enrichment results.

2.4. Construction a0nd Validation of CNV-Driven FRGs-Based Prognostic Model. To investigate whether CNV-driven FRGs were relevant to the prognosis of patients, we randomly divided the tumor samples of TCGA-LUAD into a training set ($n = 336$) and an internal validation set ($n = 143$) in the ratio of 7: 3. Firstly, the univariate Cox analysis was exploited for selecting CNV-driven FRGs associated with the overall survival (OS) of LUAD patients in the training set,

and $P < 0.05$ was considered statistical significance. Next, to further narrow down the candidate CNV-driven FRGs, we used the Least Absolute Shrinkage and Selection Operator (LASSO) algorithm to screen out the optimal gene combination for constructing the prognostic model of LUAD patients by using "glmnet" package (version 4.1-1) in the training set. Moreover, the risk score of each patient in the training set was defined as the relative expression of each genes and its associated Cox coefficient is obtained from the LASSO analysis by using the following formula:

$$\text{Riskscore} = \sum_{i=1}^{n} \text{coef}(gene_i) * \exp r(gene_i), \qquad (1)$$

where $coef(gene_i)$ is risk coefficient and $expre(gene_i)$ is expression fraction of prognostic genes. Furthermore, according to the median risk score, LUAD samples in the training set were split into the high and low-risk groups. K-M survival analysis was performed to evaluate the OS between high and low-risk groups and by using package "survminer" in R. On the other hand, the "survivalROC" package was utilized to plot receiver operating characteristic (ROC) curves to examine the prediction accuracy in prognosis prediction of LUAD patients, and the area under curve (AUC) for 1-, 2-, and 3-year OS was calculated through "survivalROC"package in R. Finally, the risk scores of LUAD samples in both internal validation set and external validation set were evaluated by using the formula and method above-mentioned, respectively.

2.5. Correlation Analysis of Risk Model and Clinical Characteristics. For further probe the relevance between the risk signature with clinical information, we compared the risk scores among LUAD patients with different clinical characteristics in the TCGA-LUAD dataset including age, stage, TNM, and smoking. The results were visualized by drawing violin plots with the "ggpubr" package (version 0.4.0) and "ggplot2" package (version 3.3.3).

2.6. Establishment and Validation of a Nomogram. The clinical characters including gender, age, T/N/M, stage, smoking, and risk score were applied to carry out a univariate Cox analysis in 479 LUAD samples, and significant factors were further enrolled in a multivariate Cox independent prognostic analysis in the TCGA-LUAD cohort. Build a prognostic nomogram to help forecast the probability of 1-, 2-, and 3-year OS for LUAD patients make use of the "rms" package. The concordance index (C-index) was employed to evaluate the accuracy of nomogram. The relationship between the predicted with observed risk for the outcomes of the nomogram was vivid displayed use calibration plots.

2.7. Immune Infiltrate Analysis. To further explore the relationship between the prognostic model and LUAD microenvironment immune infiltration, the ssGSEA was employed to calculated the immune cell scores based on the expression of 24 immune cell-related reference gene within the gene set from transcriptomic data via "gsva" package (version 1.36.3) in the 479 LUAD samples and the difference of 24 immune cell scores between the high- and low-risk groups of 479

LUAD samples. The box line plots were drawn make use of "ggplot2" package (version 3.3.3) to visualize the results of the scoring of 24 immune cells.

3. Results

3.1. Identification and Enrichment Analysis Differentially Expressed CNV Genes in LUAD. In total 1220 DEGs were present in LUAD and normal samples, of which 563 were upregulated and 657 were downregulated $(P < 0.05)$ (Figure 1(a)). PCA analysis of full sample revealed that DEGs can clearly differentiate between patients and normal samples (Figure 1(b)). The GO functional enrichment results of biological process displayed that upregulated genes were outstanding relate to nuclear division, organelle fission, and DNA conformational changes; however, the downregulated genes were remarkably interrelated with second-messenger-mediated signaling, regulation of vasculature development, and epithelial cell proliferation (Figure 1(c)). In terms of molecular function, upregulated genes were observably related to ATPase activity, antigen binding, and immunoglobulin receptor binding. The downregulated genes were significantly associated with signal receptor activator activity, cytokine receptor activity, etc. (Figure 1(d)). In terms of cell composition, upregulated genes were significantly involved in condensed nuclear chromosomes, condensed chromosomes, chromosomes, chromosomal regions, immunoglobulin complexes, etc. The downregulated genes were dramatically interrelated with collagen trimers, membrane regions, membrane microdomains, myofibrils, secretory granule membranes, and lateral plasma membranes (Figure 1(e)). KEGG enrichment results indicated that upregulated genes were observably concerned with p53 signaling pathway, alcoholism, viral carcinogenesis, bladder cancer, oocyte meiosis, and cell cycle. The downregulated genes were significantly linked with aldosterone synthesis and secretion, cell adhesion molecules, PPAR signaling pathway, and bile secretion (Figure 1(f)).

3.2. Twenty-Two CNV-Driven FRGs Were Identified and Potential Function. A total of 18224 candidate CNV driver genes were acquired in normal and tumor samples, and their distribution on 24 chromosomes is shown in Figure 2(a). Further taking the intersection of CNV driver genes and DEGs, we identified 251 upregulated CNV driver genes and 231 downregulated CNV driver genes. Finally, this study identified 22 differential CNV-driven FRGs on account of 397 FRGs and differentially expressed CNV driver genes. These genes are predominantly correlated with cellular response to chemical stress, reactive oxygen species metabolic process, response to oxidative stress, and cellular response to oxidative stress (Figure 2(b)) and notably associated with cysteine and methionine metabolism, malaria, biosynthesis of amino acids, and HIF-1 signaling pathway $(P < 0.05)$ (Figure 2(c)).

3.3. Establishment and Validation of the Six CNV-Driven FRG Signature. After univariate Cox regression analysis, seven CNV-driven FRGs were authenticated as candidate prognosis genes in the TCGA-LUAD training set (Figure 3(a)). And a 6-gene signature was finally set up based on the optimum λ

(a)

(b)

(c)

(d)

(e)

(f)

Figure 1: Screening and enrichment analysis of differentially expressed genes (DEGs) in LUAD. (a) Volcano map of DEGs. (b) Principal component analysis (PCA) based on DEGs in TCGA-LUAD sample. Bar graph of the most enrichment GO terms for DEGs, including GO-BP (c), GO-CC (d), and GO-MF (e). (f) Bar graph of the most enrichment KEGG pathways for DEGs.
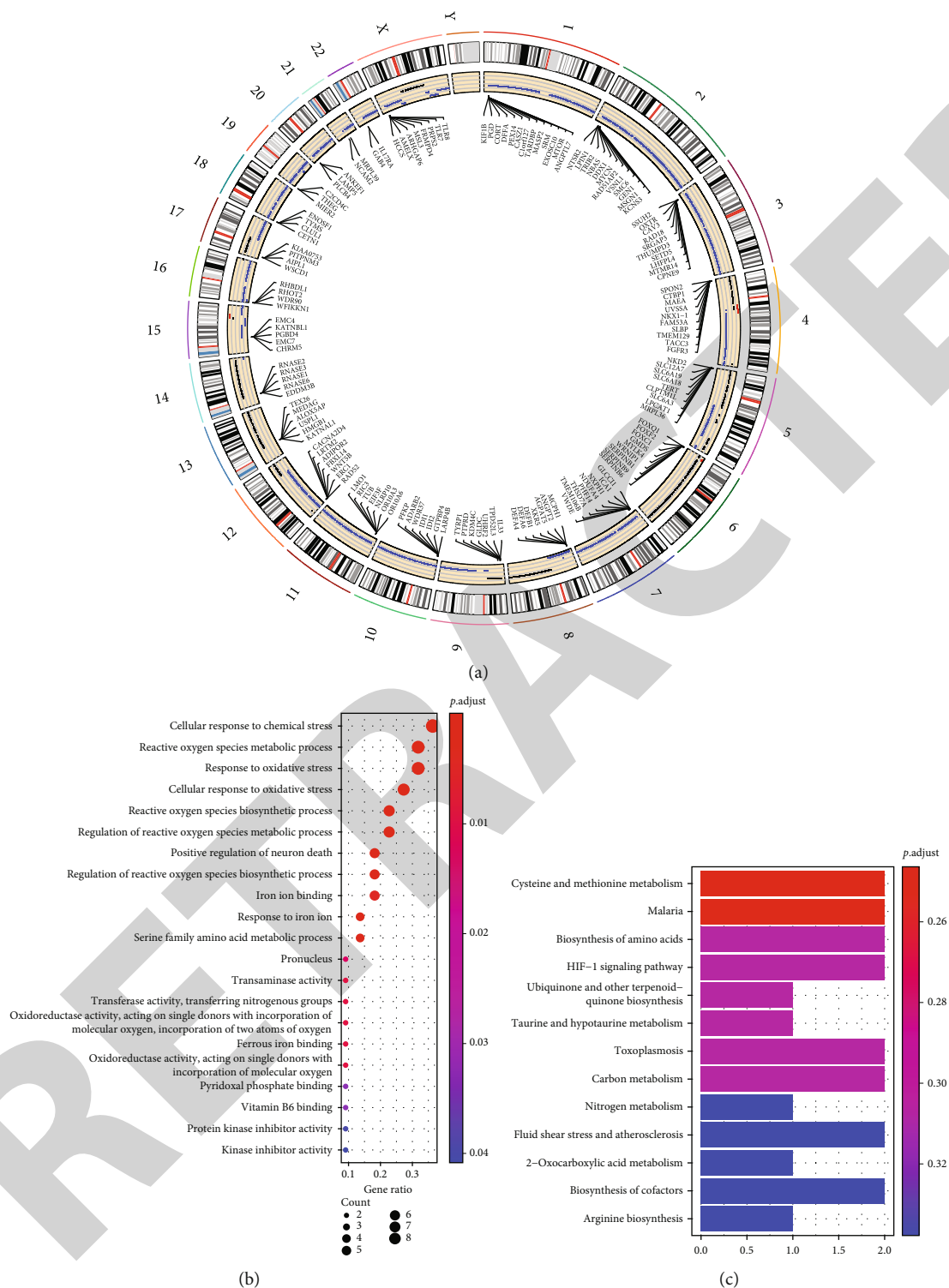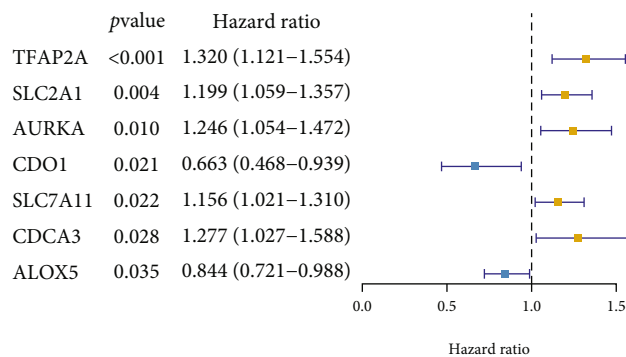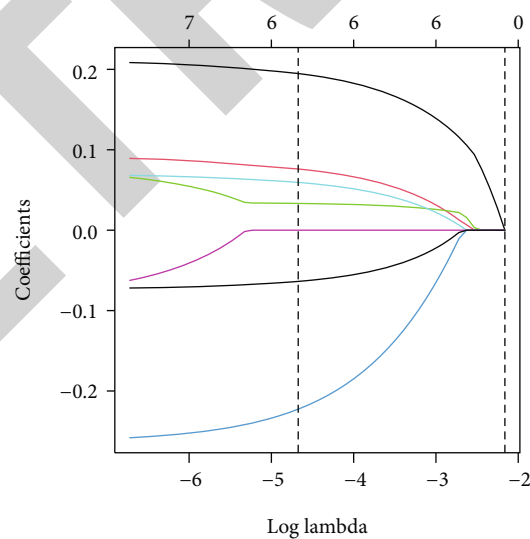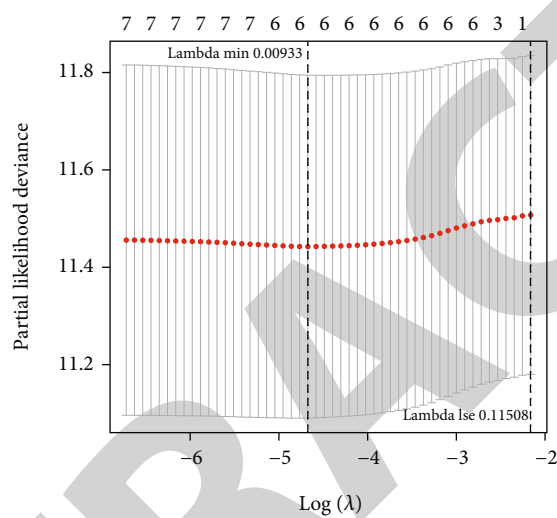
(a)

(b)

(c)

FIGURE 2: Screening for differential CNV driver genes in TCGA-LUAD. (a) The outer circle represents 24 chromosomes, including sex chromosomes. The inner circle represents the distribution of CNV (blue dots represent CNV absence). (b) Bubble chart of the GO enrichment analysis of the CNV-driven ferroptosis-related genes. (c) Bars chart of the KEGG pathway analysis of the CNV-driven ferroptosis-related genes.

value 0.00933 after executed LASSO regression (Figure 3(b)). The RiskScore = $0.20719 \times$ TFAP2A + $0.08626 \times$ SLC2A1 + $0.03424 \times$ AURKA + $0.06759 \times$ SLC7A11 + $(-0.26359) \times$ CDO1 + $(-0.07202) \times$ ALOX5. On the grounds of the opti-

mal truncation risk score 0.97, LUAD samples were segmented into high- and low-risk groups, also patients with higher risk with shorter survival time (Figure 3(c)). K-M analyses manifested that high-risk patients had worse

	$p$value	Hazard ratio
TFAP2A	<0.001	1.320 (1.121−1.554)
SLC2A1	0.004	1.199 (1.059−1.357)
AURKA	0.010	1.246 (1.054−1.472)
CDO1	0.021	0.663 (0.468−0.939)
SLC7A11	0.022	1.156 (1.021−1.310)
CDCA3	0.028	1.277 (1.027−1.588)
ALOX5	0.035	0.844 (0.721−0.988)

Hazard ratio

(a)

(b)

Figure 3: Continued.

(c)

(d)

(e)

FIGURE 3: Continued.

(f)

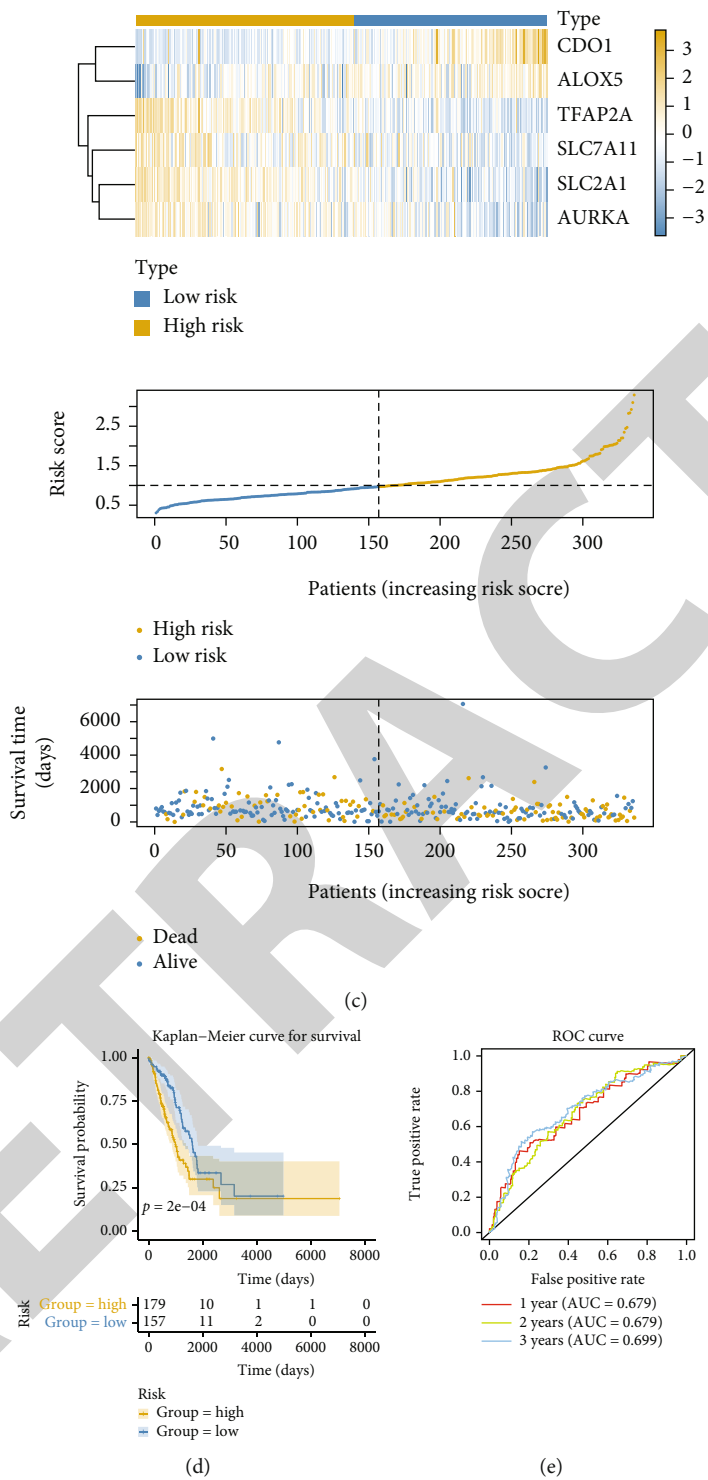(g)   (h)
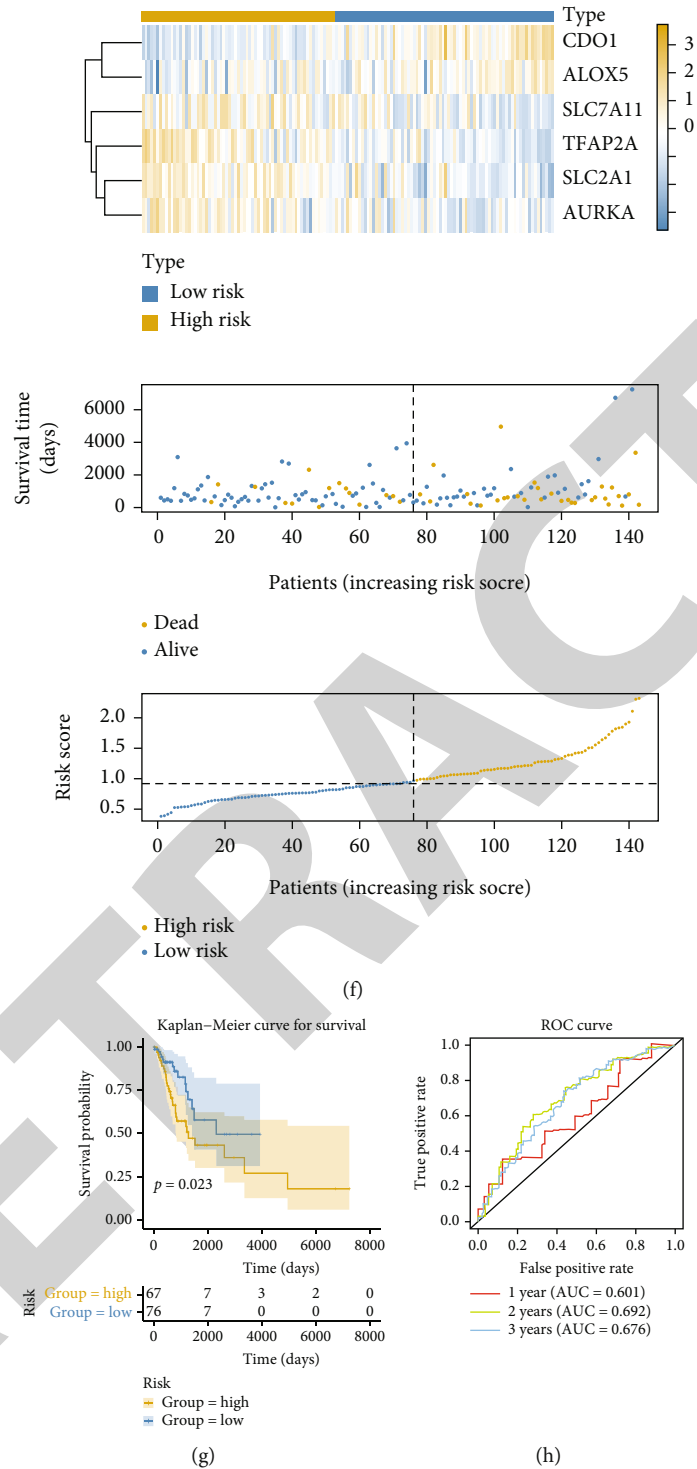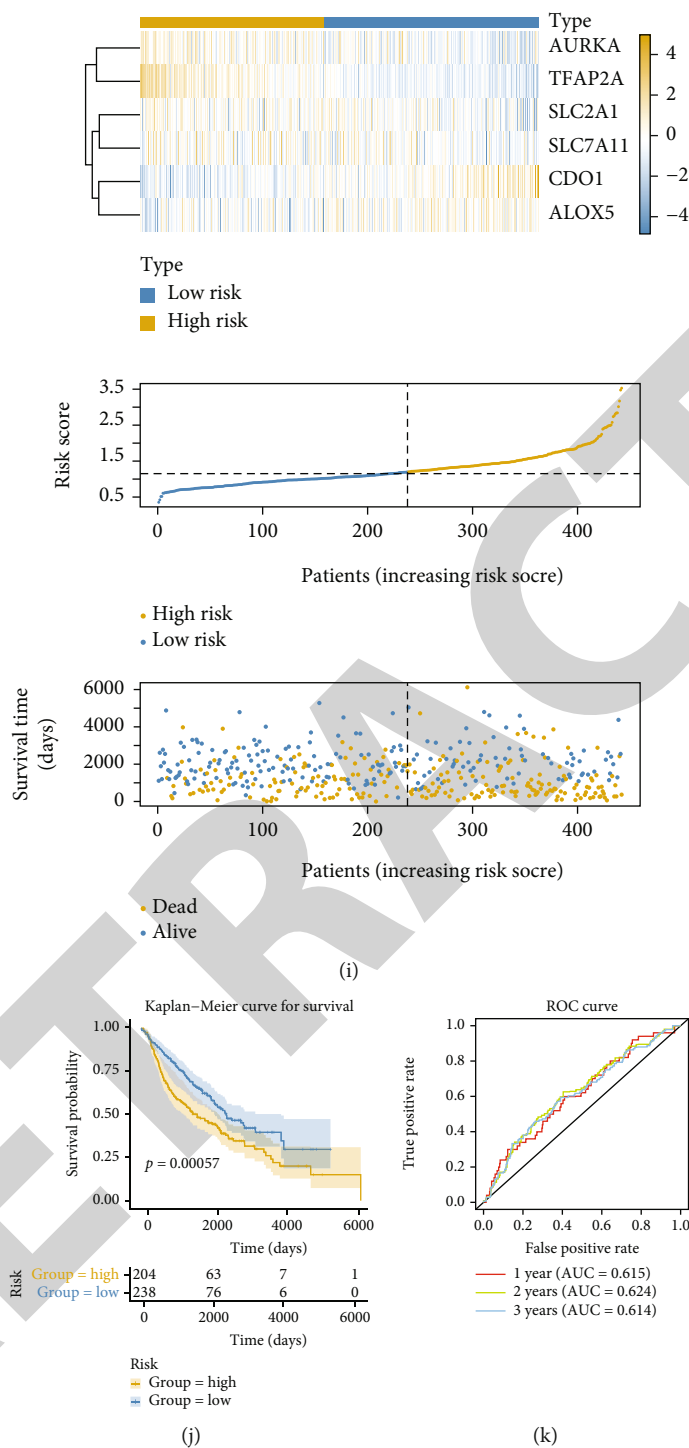
FIGURE 3: Continued.

Figure 3: CNV-driven ferroptosis-related genes are associated with LUAD prognosis. (a) Forest map of CNV-driven ferroptosis-related genes by univariate Cox regression. Yellow: risk factors; blue: protective factors. (b) The LASSO Cox analysis identified regression coefficient and 6 genes most correlated with prognostics. (c) Risk curve, scatter plot, and risk model gene expression heat map of high and low risk grouping of LUAD patients in the training set. (d) Survival curves of the high and low risk grouping of LUAD patients in the training set. (e) ROC curve for predicting the 1-, 2-, and 3-year OS of LUAD patients in the training set. The area below the curve is called AUC (area under curve) and is used to indicate prediction accuracy and sensitivity. The higher the AUC value, the larger the area below the curve, the higher the prediction accuracy. (f) Risk curves, scatter plots, and model gene expression heat map of high and low risk group in the internal validation set. (g) Survival curves for high and low risk grouping in internal validation set. (h) ROC curve for predicting the 1-, 2-, and 3-year OS in internal validation set. (i) Risk curves, scatter plots, and model gene expression heat map of high and low risk group in the GSE68465. (j) Survival curves for high- and low-risk group in the GSE68465. (k) ROC curve for predicting the 1-, 2-, and 3-year OS of LUAD patients in the GSE68465.
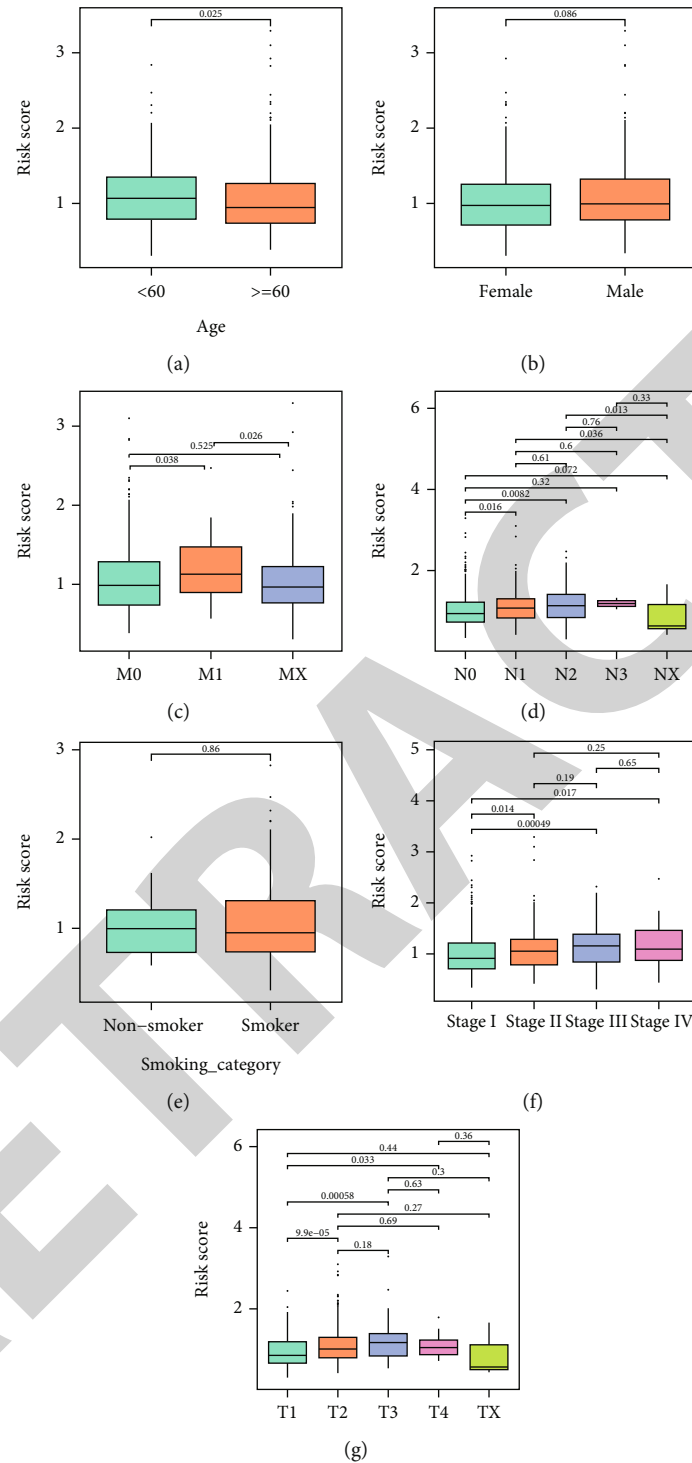
Figure 4: The risk scores in different clinical subgroups of LUAD patients. (a) age; (b) gender; (c) M-stage; (d) N-stage; (e) smoking category; (f) stage; and (g) T-stage.

survival (Figure 3(d)). The 1-, 3-, and 5-year AUC values in the TCGA cohort were 0.679, 0.679, and 0.669, (Figure 3(e)). In the internal validation set TCGA-LUAD, patients were classified into high/low risk groups on the basis of the optimal threshold of risk score 0.97; also, the high-risk score group had a worse survival rate ($P = 0.023$) (Figures 3(f)–3(g)). In addition, ROC curve results showed AUC values

exceed 0.6 at 1, 3, and 5 years (Figure 3(h)). Similar outcomes were verified in the external validation set GSE68465 (Figures 3(i)–3(k)).

3.4. *Correlation between Prognostic Model and Clinical Characteristics.* Correlation analysis of prognostic models and clinical factors revealed that risk scores were
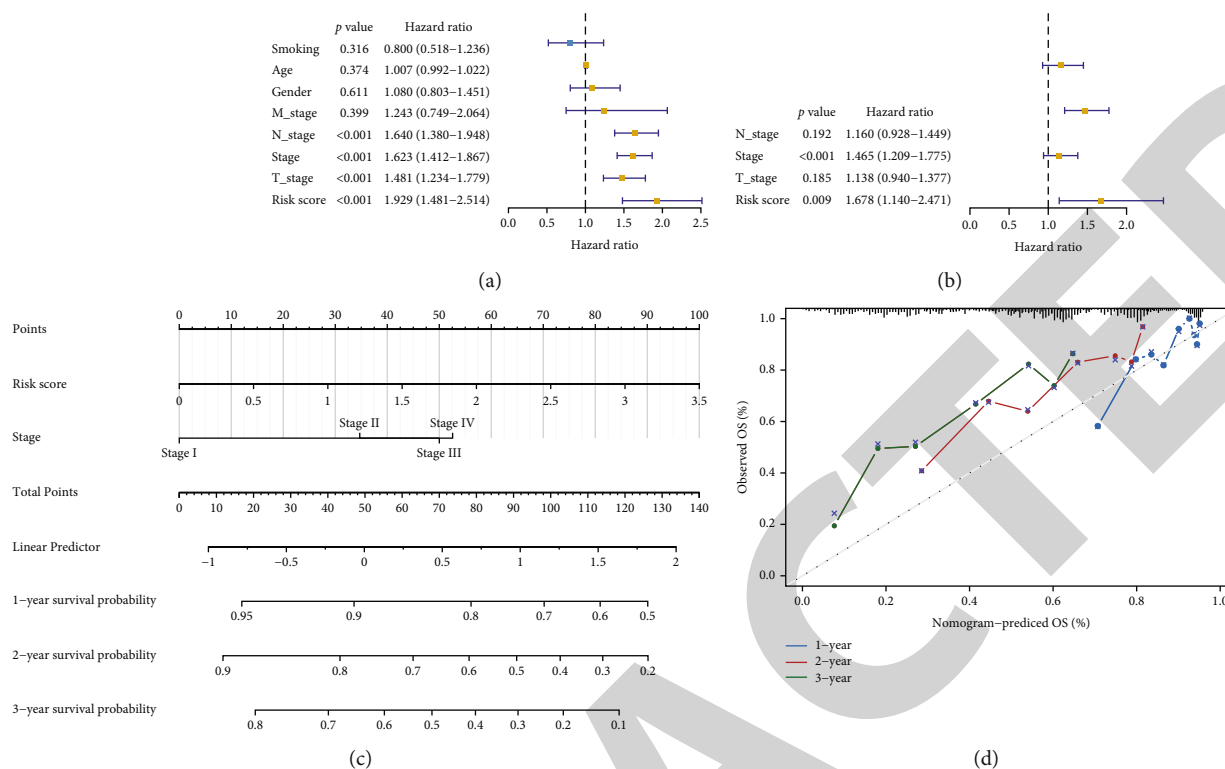
FIGURE 5: Independent prognostic factor analysis and Nomogram construction. (a) Forest map of univariate Cox analysis of clinical characteristics. (b) Forest map of multivariate Cox analysis. (c) Nomogram for predicting the 1-, 2-, and 3-year survival rates of LUAD patients. (d) Correctional curve of the nomogram.

significantly correlated with T/N and stage. The risk scores of T2 and T3 patients were statistically noteworthy over top those of T1 patients. The risk scores of N1, N2, and N3 patients were higher than N0 patients. And risk scores of stage II and stage III patients were higher than stage I patients ($P < 0.05$) (Figure 4).

3.5. Construction of the Nomogram.
To evaluate prognostic feature with clinical feasibility of the risk model, then the univariate with multivariate analyses were utilized to decide the independent prognostic element, as well as the nomogram was exploited. After Cox regression analysis, the stage with risk score were recognized as independent prognostic element ($P = 0.001$ and 0.009, respectively) (Figures 5(a) and 5(b)). A prediction nomogram was established to forecast 1-, 2-, and 3-year outcomes of LUAD cases (Figures 5(c) and 5(d)).

3.6. Immune Infiltration Landscape in Different Risk Groups.
By ssGSEA, the result obtained 24 immune cells score or each LUAD patient, as shown in Figure 6(a). Further analysis of the variation in immune cell infiltration between the high-/low-risk groups revealed that all 19 cells were notably variation in two groups, including DC, iDC, pDC, Mast cells, Th2 cells, CD8 T cells, eosinophils, cytotoxic cells, Tgd, TFH, macrophages, T cells, NK cells, Tem, Tcm, B cells, T helper cells, NK CD56dim cells, and NK CD56bright cells ($P < 0.05$) (Figure 6(b)).

4. Discussion

Ferroptosis is a novel mode of cell death that is mainly triggered by the amassing of ROS and LPO causing fatal cell damage. The induction mechanism of ferroptosis in tumor cells can be broadly divided into classical and non-classical pathways. The former is through restrain of the cystine/glutamate antiporter system- (System Xc-) glutathione- (GSH-) GPX4 axis, resulting in the amassing of ROS for induces ferroptosis, while the latter causes ferroptosis directly or indirectly by the iron metabolism and mitochondria. In recent years, research finding ferroptosis possesses an integral effect for proliferation with lung cancer apoptosis [16–19]. Hence, it is rational to conjecture that FRGs may also play a part in predicting the survival outcome of LUAD and provide reference for clinical identification of ideal prognostic markers.

In our study, tall 22 differentially expressed CNV-driven FRGs were acquired in LUAD based on bioinformation technology. These genes were significantly associated with serine family amino acid metabolism, iron regulation, reactive oxygen species metabolism, and cellular response to oxidative stress, and were also involved in amino acid metabolism, malaria, amino acid biosynthesis, and HIF-1 signaling pathways. Wan et al. [20] confirmed that following hyperthermia, the HIF-1α, part of HIF-1, has the potential to induce proliferation and angiogenesis in residual NSCLC with SCLC. The carbon metabolic showed to meet the tumor
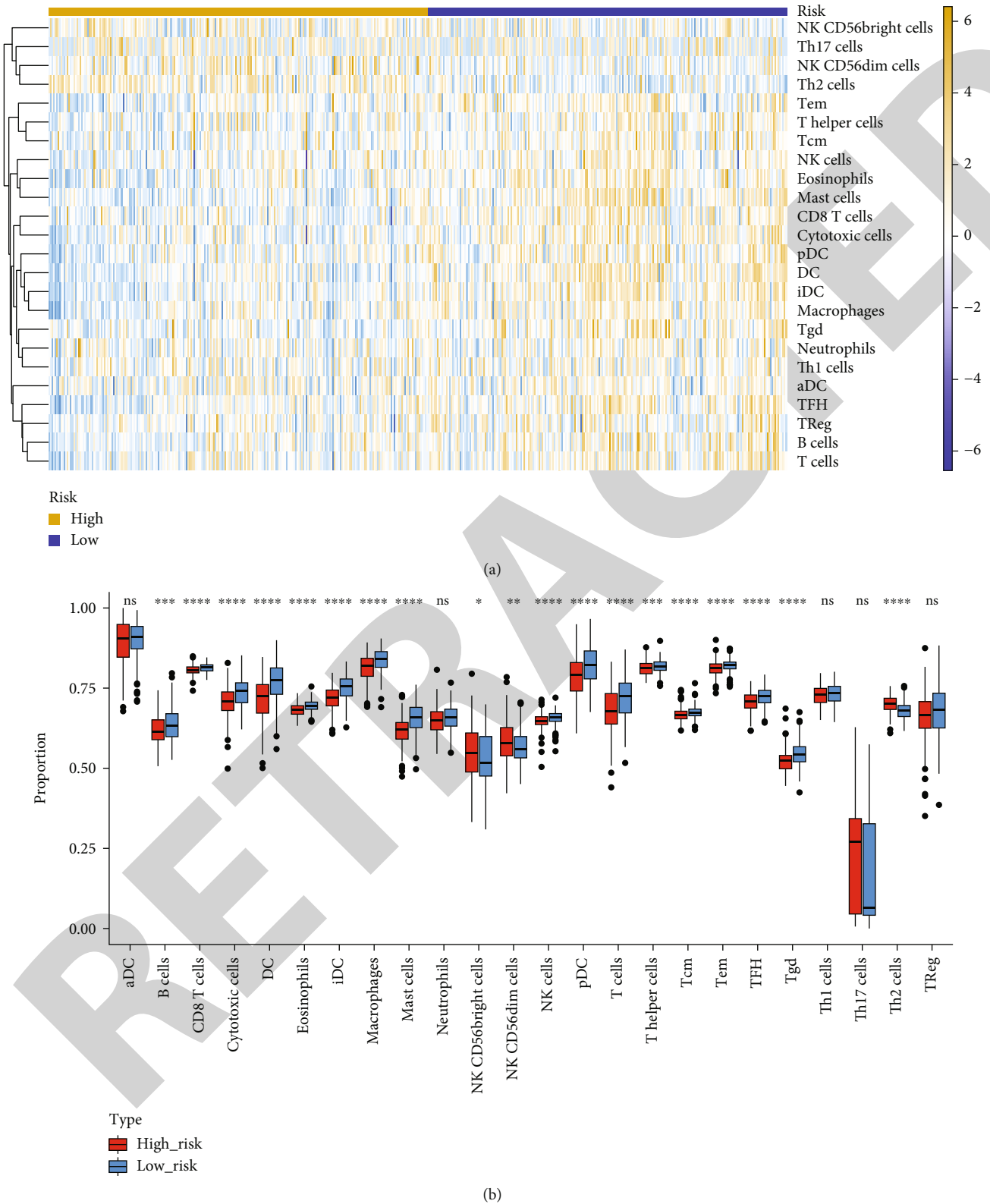
(a)

(b)

Figure 6: Differential analysis of immune cell infiltration. (a) Heat map of ssGSEA scores of 24 immune cells. ssGSEA: single-sample gene set enrichment analysis. (b) Boxplot of immune cell differences between the high and low risk groups. $^*P < 0.05$ and $^{**}P < 0.01$.

specific nutrient requirements in the proliferation of LUAD [21]. Moreover, Yao et al. [22] exposed that LUAD has a stronger dependence on 1CM activity than SQCLC or SCLC.

Based on the relevant file of LUAD-TCGA and GEO database, we structured a prognostic feature formed of six genes, including TFAP2A, SLC2A1, AURKA, CDO1,

SLC7A11, and ALOX5, through a series of bioinformatics techniques. Among them, TFAP2A, SLC2A1, AURKA, and SLC7A11 are risk factors for survival in LUAD, while CDO1 and ALOX5 are protective factors. It was reported that CDO1 showed tumor suppressive activity both in cell and mouse model experiment [23]. ALOX5 suppressed tumor growth in KrasG12D mice through its enzyme product AT-RvD1 [24]. In addition, Inhibition of ALOX5 gene can promote the growth of lung cancer [25]. TFAP2A is also known as ap-2A that is mainly referred to the regulation of embryonic development, proliferation, apoptosis, and stem cell differentiation [26]. TFAP2A can negatively modulate ferroptosis by activating the NRF2 [27]. In the prognostic model of LUAD of 15 FRGs constructed by Guang xu Tu et al. [28]. SLC2A1 is a glucose transport protein coding gene that controls the absorption of glucose, and the encoded protein is closely related to glucose metabolism. SLC2A1 is connected with tumor progression and metastasis [29] that upregulated with poorer prognosis, including in LUAD [30]. AURKA is a recognized tumor susceptibility gene, which is essential for the normal process of cell mitosis [31] and overexpressed in many cancers and consists of breast cancer [32], colorectal cancer [33], gastrointestinal cancer [34], bladder cancer [35], and lung cancer [36]. Recent studies indicated that AURKA is related to poor prognosis in LUAD [37, 38]. The main function of CDO1, a metalloproteinase, is involved in cysteine regulation and taurine synthesis. Hao et al. [39] confirmed that suppression of CDO1 can restore GSH levels with prevent ROS produce, thus inhibiting ferroptosis. Studies have found that hypermethylation of CDO1 promoter region is common in NSCLC and it is believed that the methylation of CDO1 has certain specificity for NSCLC [40, 41]. The inhibition of SLC7A11-mediated cystine uptake results in intracellular glutathione deficiency, leading to ferroptosis-mediated cell death [7]. Xuan et al. [30] reported that upregulated SLC7A11 was shown in NSCLC patients and is related to worse prognosis. ALOX5 is an initiation enzyme that mainly mediates the production of inflammatory mediators leukotriene and lipoxin. ALOX5 can inhibit drug-induced ferroptosis through overexpression [42]. ALOX5 research has been carried out on number of cancers, such as glioblastoma [43], breast cancer [44], and lung cancer [42].

In this study, 479 luad patients were divided into high-risk group and low-risk group, of which the high-risk group had a poor prognosis. Subsequent independent prognostic analysis found that risk score was a trustworthy independent element. Furthermore, a nomogram with excellent predictive performance was developed for forecasting the outcome of LUAD patients at 1, 2, and 3 years. The nomogram has good predictive ability.

Immunotherapy is a research hotspot in recent years, and understanding the prognostic relationship between immune infiltration and LUAD may contribute to the development of LUAD treatment. By ssGSEA, this study obtained a score of 24 immune cells for LUAD samples. Further analysis of the variation in immune cell distribution in two groups revealed that a total of 19 cells were outstanding variation between different risk groups, which demonstrate that the prognosis of LUAD was interrelated to immune infiltration. Many studies confirmed the relevance between the immune cell with the clinical outcome of lung cancer. Bao et al. [45] revealed that masses of mast cells be something to do with better survival in patients with early-stage LUAD. The same conclusion was reached in this study. In contrast, Lilis et al. [46] found that mast cells are associated with LUAD progression. It was reported that CD8+ T cell density was one of the prognostic factors of bad prognosis for LUAD patients [47]. Nevertheless, contrary result was obtained in this study. Another study revealed that IL-38 promoted LUAD proliferation by restraining of CD8+ T lymphocytes in the tumor microenvironment [48]. In addition, through comparative analysis, macrophages and pDC were found to be higher in the low-risk population in our analysis. This finding suggested that macrophages and pDC were associated with better prognosis of lung adenocarcinoma, which was in contrast to previous studies. Jung et al. [49] found that cancers with higher tumor associated macrophage densities were associated with awful survival outcomes. Rega et al. [50] demonstrated that pDC knockout inhibited tumor propagation of low-dose lPS-treated mice. To sum up, different researchers have different views. The prognostic role and mechanism of differential immune cells in this study of lung adenocarcinoma need to be further studied.

5. Conclusion

In conclusion, the six CNV-driven ferroptosis-related gene composition prognostic models screened by a variety of bioinformatics methods have good prognostic value for LUAD and may provide certain basis for individual treatment and evaluation of LUAD patients. However, this study has certain limitations that the specific mechanism of the effect of CNV-driven FRGs on LUAD still needs to be further verified by basic experiments. We will continue to focus on the research dynamic these genes.

Data Availability

The datasets generated during and/or analyzed during the current study are available from the corresponding author on reasonable request.

Conflicts of Interest

The authors declare that there is no conflict of interest regarding the publication of this paper.

Acknowledgments

Supplementary Materials

A comprehensive literature survey about ferroptosis was performed, and high-quality articles were retrieved, in which 60 ferroptosis-related genes were identified and are presented in Supplementary file 1. (*Supplementary Materials*)

References

[1] R. L. Siegel, K. D. Miller, and A. Jemal, "Cancer statistics, 2018," *CA: a Cancer Journal for Clinicians*, vol. 68, no. 1, pp. 7–30, 2018.

[2] S. Blandin Knight, P. A. Crosbie, H. Balata, J. Chudziak, T. Hussell, and C. Dive, "Progress and prospects of early detection in lung cancer," *Open Biology*, vol. 7, no. 9, 2017.

[3] T. V. Denisenko, I. N. Bunkerish, and B. Zhivotovsky, "Cell death-based treatment of lung adenocarcinoma," *Cell Death & Disease*, vol. 9, no. 2, p. 117, 2018.

[4] R. L. Siegel, K. D. Miller, and A. Jemal, "Cancer statistics, 2019," *CA: a Cancer Journal for Clinicians*, vol. 69, no. 1, pp. 7–34, 2019.

[5] T. Hensing, A. Chawla, R. Batra, and R. Salgia, "A personalized treatment for lung cancer: molecular pathways, targeted therapies, and genomic characterization," *Advances in Experimental Medicine and Biology*, vol. 799, pp. 85–117, 2014.

[6] S. J. Dixon, K. M. Lemberg, M. R. Lamprecht et al., "Ferroptosis: an iron-dependent form of nonapoptotic cell death," *Cell*, vol. 149, no. 5, pp. 1060–1072, 2012.

[7] B. R. Stockwell, J. P. Friedmann Angeli, H. Bayir et al., "Ferroptosis: a regulated cell death nexus linking metabolism, redox biology, and disease," *Cell*, vol. 171, no. 2, pp. 273–285, 2017.

[8] L. Jiang, N. Kon, T. Li et al., "Ferroptosis as a p53-mediated activity during tumour suppression," *Nature*, vol. 520, no. 7545, pp. 57–62, 2015.

[9] X. Chen, R. Kang, G. Kroemer, and D. Tang, "Broadening horizons: the role of ferroptosis in cancer," *Nature Reviews. Clinical Oncology*, vol. 18, no. 5, pp. 280–296, 2021.

[10] J. Ni, K. Chen, J. Zhang, and X. Zhang, "Inhibition of GPX4 or mTOR overcomes resistance to lapatinib via promoting ferroptosis in NSCLC cells," *Biochemical and Biophysical Research Communications*, vol. 567, pp. 154–160, 2021.

[11] K. Inaki and E. T. Liu, "Structural mutations in cancer: mechanistic and functional insights," *Trends in Genetics*, vol. 28, no. 11, pp. 550–559, 2012.

[12] D. F. Conrad, D. Pinto, R. Redon et al., "Origins and functional impact of copy number variation in the human genome," *Nature*, vol. 464, no. 7289, pp. 704–712, 2010.

[13] K. Czubak, M. A. Lewandowska, K. Klonowska et al., "High copy number variation of cancer-related microRNA genes and frequent amplification of DICER1 and DROSHA in lung cancer [J]," *Oncotarget*, vol. 6, no. 27, pp. 23399–23416, 2015.

[14] K. B. Sriram, J. E. Larsen, S. M. Savarimuthu Francis et al., "Array-comparative genomic hybridization reveals loss of SOCS6 is associated with poor prognosis in primary lung squamous cell carcinoma," *PLoS One*, vol. 7, no. 2, article e30398, 2012.

[15] L. Liu, J. Huang, K. Wang et al., "Identification of hallmarks of lung adenocarcinoma prognosis using whole genome sequencing," *Oncotarget*, vol. 6, no. 35, pp. 38016–38028, 2015.

[16] S. W. Alvarez, V. O. Sviderskiy, E. M. Terzi et al., "NFS1 undergoes positive selection in lung tumours and protects cells from ferroptosis," *Nature*, vol. 551, no. 7682, pp. 639–643, 2017.

[17] B. Hassannia, B. Wiernicki, I. Ingold et al., "Nano-targeted induction of dual ferroptotic mechanisms eradicates high-risk neuroblastoma," *The Journal of Clinical Investigation*, vol. 128, no. 8, pp. 3341–3355, 2018.

[18] Y. Lai, Z. Zhang, J. Li et al., "STYK1/NOK correlates with ferroptosis in non-small cell lung carcinoma," *Biochemical and Biophysical Research Communications*, vol. 519, no. 4, pp. 659–666, 2019.

[19] X. M. Ji, J. Qian, S. M. J. Rahman et al., "xCT (SLC7A11)-mediated metabolic reprogramming promotes non-small cell lung cancer progression," *Oncogene*, vol. 37, no. 36, pp. 5007–5019, 2018.

[20] J. Wan and W. Wu, "Hyperthermia induced HIF-1a expression of lung cancer through AKT and ERK signaling pathways," *Journal of Experimental & Clinical Cancer Research*, vol. 35, no. 1, p. 119, 2016.

[21] B. Zhang, A. Zheng, P. Hydbring et al., "PHGDH defines a metabolic subtype in lung adenocarcinomas with poor prognosis," *Cell Reports*, vol. 19, no. 11, pp. 2289–2303, 2017.

[22] S. Yao, L. Peng, O. Elakad et al., "One carbon metabolism in human lung cancer," *Translational lung Cancer Research*, vol. 10, no. 6, pp. 2523–2538, 2021.

[23] M. Brait, S. Ling, J. K. Nagpal et al., "Cysteine dioxygenase 1 is a tumor suppressor gene silenced by promoter methylation in multiple human cancers," *PLoS One*, vol. 7, no. 9, article e44951, 2012.

[24] S. Bozinovski, "Aspirin-triggered resolvin D1 reduces proliferation and the neutrophil to lymphocyte ratio in a mutant KRAS-driven lung adenocarcinoma model," *Cancers*, vol. 13, no. 13, article 3224, 2021.

[25] J. M. Poczobutt, T. T. Nguyen, D. Hanson et al., "Deletion of 5-lipoxygenase in the tumor microenvironment promotes lung cancer progression and metastasis through regulating T cell recruitment," *The Journal of Immunology*, vol. 196, no. 2, pp. 891–901, 2016.

[26] E. Van Otterloo, H. Li, K. L. Jones, and T. Williams, "AP-2α and AP-2β cooperatively orchestrate homeobox gene expression during branchial arch patterning," *Development*, vol. 145, no. 2, 2017.

[27] H. X. Huang, G. Yang, Y. Yang, J. Yan, X. Y. Tang, and Q. Pan, "TFAP2A is a novel regulator that modulates ferroptosis in gallbladder carcinoma cells via the Nrf 2 signalling axis," *European Review for Medical and Pharmacological Sciences*, vol. 24, no. 9, pp. 4745–4755, 2020.

[28] G. Tu, W. Peng, Q. Cai et al., "Construction and validation of a 15-gene ferroptosis signature in lung adenocarcinoma," *PeerJ*, vol. 9, article e11687, 2021.

[29] W. Guo, S. Sun, L. Guo et al., "Elevated SLC2A1 expression correlates with poor prognosis in patients with surgically resected lung adenocarcinoma: a study based on Immunohistochemical analysis and bioinformatics," *DNA and Cell Biology*, vol. 39, no. 4, pp. 631–644, 2020.

[30] J. Zhu, Y. Mou, S. Ye et al., "Identification of a six-gene SLC family signature with prognostic value in patients with lung adenocarcinoma," *Frontiers in cell and developmental biology*, vol. 9, article 803198, 2021.

[31] N. J. Taylor, J. T. Bensen, C. Poole et al., "Genetic variation in cell cycle regulatory gene AURKA and association with

intrinsic breast cancer subtype," *Molecular Carcinogenesis*, vol. 54, no. 12, pp. 1668–1677, 2015.

[32] H. J. Donnella, J. T. Webber, R. S. Levin et al., "Kinome rewiring reveals AURKA limits PI3K-pathway inhibitor efficacy in breast cancer," *Nature Chemical Biology*, vol. 14, no. 8, pp. 768–777, 2018.

[33] C. Wu, J. Lyu, E. J. Yang, Y. Liu, B. Zhang, and J. S. Shim, "Targeting AURKA-CDC25C axis to induce synthetic lethality in ARID1A-deficient colorectal cancer cells," *Nature Communications*, vol. 9, no. 1, p. 3212, 2018.

[34] L. Wang-Bishop, Z. Chen, A. Gomaa et al., "Inhibition of AURKA reduces proliferation and survival of gastrointestinal cancer cells with activated KRAS by preventing activation of RPS6KB1," *Gastroenterology*, vol. 156, no. 3, pp. 662–675.e7, 2019.

[35] M. Guo, S. Lu, H. Huang et al., "Increased AURKA promotes cell proliferation and predicts poor prognosis in bladder cancer," *BMC Systems Biology*, vol. 12, no. S7, p. 118, 2018.

[36] M. Y. Zhang, X. X. Liu, H. Li, R. Li, X. Liu, and Y. Q. Qu, "Elevated mRNA levels of AURKA, CDC20 and TPX2 are associated with poor prognosis of smoking related lung adenocarcinoma using bioinformatics analysis," *International Journal of Medical Sciences*, vol. 15, no. 14, pp. 1676–1685, 2018.

[37] B. Deb, P. Sengupta, J. Sambath, and P. Kumar, "Bioinformatics analysis of global proteomic and phosphoproteomic data sets revealed activation of NEK2 and AURKA in cancers," *Biomolecules*, vol. 10, no. 2, p. 237, 2020.

[38] M. Zhang, C. Huo, Y. Jiang et al., "AURKA and FAM83A are prognostic biomarkers and correlated with tumor-infiltrating lymphocytes in smoking related lung adenocarcinoma," *Journal of Cancer*, vol. 12, no. 6, pp. 1742–1754, 2021.

[39] S. Hao, J. Yu, W. He et al., "Cysteine dioxygenase 1 mediates erastin-induced ferroptosis in human gastric cancer cells," *Neoplasia*, vol. 19, no. 12, pp. 1022–1032, 2017.

[40] W. A. Pan, Z. H. Honglin, S. H. Ruifeng et al., "The role of plasma CDO1 methylation in the early diagnosis of lung cancer," *Zhongguo fei ai za zhi = Chinese journal of lung cancer*, vol. 23, no. 5, 2020.

[41] L. Li, Z. Ye, S. Yang et al., "Diagnosis of pulmonary nodules by DNA methylation analysis in bronchoalveolar lavage fluids," *Clinical Epigenetics*, vol. 13, no. 1, p. 185, 2021.

[42] X. Wei, C. Wang, H. Feng et al., "Effects of ALOX5, IL6R and SFTPD gene polymorphisms on the risk of lung cancer: a case-control study in China," *International Immunopharmacology*, vol. 79, article 106155, 2020.

[43] J. Tian-Bo, L. Xiao-Lan, Y. Hua et al., "Association of polymorphisms in FLT3, EGFR, ALOX5, and NEIL3 with glioblastoma in the Han Chinese population," *Medical Oncology*, vol. 30, no. 4, p. 718, 2013.

[44] X. Zhou, Y. Jiang, Q. Li, Z. Huang, H. Yang, and C. Wei, "Aberrant ALOX5 activation correlates with HER2 status and mediates breast cancer biological activities through multiple mechanisms," *BioMed Research International*, vol. 2020, Article ID 1703531, 8 pages, 2020.

[45] X. Bao, R. Shi, T. Zhao, and Y. Wang, "Mast cell-based molecular subtypes and signature associated with clinical outcome in early-stage lung adenocarcinoma," *Molecular Oncology*, vol. 14, no. 5, pp. 917–932, 2020.

[46] I. Lilis, G. Ntaliarda, V. Papaleonidopoulos et al., "Interleukin-1β provided by KIT-competent mast cells is required for KRAS-mutant lung adenocarcinoma," *Oncoimmunology*, vol. 8, no. 7, pp. 1–18, 2019.

[47] T. K. Kilvaer, E. E. Paulsen, S. Andersen et al., "Digitally quantified CD8+ cells: the best candidate marker for an immune cell score in non-small cell lung cancer?," *Carcinogenesis*, vol. 41, no. 12, pp. 1671–1681, 2020.

[48] F. Kinoshita, T. Tagawa, T. Akamine et al., "Interleukin-38 promotes tumor growth through regulation of CD8+ tumor-infiltrating lymphocytes in lung cancer tumor microenvironment," *Cancer Immunology, Immunotherapy*, vol. 70, no. 1, pp. 123–135, 2021.

[49] K. Y. Jung, S. W. Cho, Y. A. Kim et al., "Cancers with higher density of tumor-associated macrophages were associated with poor survival rates," *Journal of Pathology and Translational Medicine*, vol. 49, no. 4, pp. 318–324, 2015.

[50] A. Rega, M. Terlizzi, A. Luciano et al., "Plasmacytoid dendritic cells play a key role in tumor progression in lipopolysaccharide-stimulated lung tumor-bearing mice," *Journal of Immunology*, vol. 190, no. 5, pp. 2391–2402, 2013.